Contrib Mineral Petrol (2006) 152: 111–124
DOI 10.1007/s00410-006-0097-0

ORIGINAL PAPER

B. E. Mordick · A. F. Glazner

Clinopyroxene thermobarometry of basalts from the Coso and Big Pine volcanic fields, California

Received: 14 June 2005 / Accepted: 17 March 2006 / Published online: 5 May 2006

Abstract The Coso and Big Pine volcanic fields of eastern California exhibit different magmatic histories. The Big Pine field erupted only basalt lavas, some of which bear mantle xenoliths, whereas the Coso field erupted both basalt and rhyolite and is a major geothermal resource. These different magmatic products could be explained if Coso basalts stalled in the crust before erupting, providing heat to generate silicic magma, whereas Big Pine basalts erupted directly from mantle depths. Clinopyroxene–liquid thermobarometry indicates an average clinopyroxene crystallization depth of 45 km for Big Pine basalts and 19 km for Coso basalts, consistent with this hypothesis. Differences in crustal density, crustal structure, and prior magmatic history may have contributed to the different magmatic processes operating at each field. Our results indicate that the effects of analytical error, crystal zoning, and correlated errors on estimated temperatures and pressures from the thermobarometer are relatively small compared to intersample differences.

Introduction

It is unclear why some basaltic volcanic fields produce rhyolitic magma and others do not. This is an important distinction to make because rhyolite magma bodies are often associated with geothermal activity, such as at the Coso geothermal area in eastern California (Fig. 1). Both basalt and rhyolite occur in the Coso volcanic field, where there is a large geothermal resource. The nearby Big Pine volcanic field, located approximately 120 km north of the Coso field in Owens Valley, is dominated by basalt and shows no signs of a geothermal resource. Volcanism in both areas is associated with extension of the Basin and Range province (Bacon 1982; Ormerod et al. 1988, 1991) yet it is clear from the chemical diversity of erupted lavas that different magmatic processes operate in each field.

Mafic magma must stall in the crust to generate silicic and intermediate magmas. The absence of rhyolite at Big Pine would suggest that basaltic magma did not stall in the crust, but rather erupted directly from mantle melting depths. Consequently, Big Pine basalts should record deep crystallization of phenocrysts. Conversely, current hypotheses suggest that Coso basalts stalled in the crust before erupting, providing a heat source to generate silicic magmas (Bacon 1982; Bacon and Metz 1984; Manley and Bacon 2000). If this hypothesis is correct then Coso basalts should record greater crystallization depths than Coso rhyolites and shallower crystallization depths than Big Pine basalts, reflecting the depth of storage and silicic melt generation.

We use the clinopyroxene–liquid thermobarometer of Putirka et al. (1996) to determine the depths of pyroxene crystallization of Coso and Big Pine basalts in order to test two hypotheses: (1) that mantle xenolith-bearing basalts from the Big Pine volcanic field, which lack associated rhyolite, crystallized at greater depths than basalts from the Coso volcanic field, which erupted with abundant rhyolite; and (2) that Coso basaltic magma was stored at greater depths than Coso rhyolitic magma. We also evaluate the precision of the thermobarometer, how analytical error propagates through the equations to produce correlated P–T arrays, how sensitive the thermobarometer is to zoning (both core-to-rim and

Electronic Supplementary Material Supplementary material is available for this article at http://dx.doi.org/10.1007/s00410-006-0097-0 and is accessible for authorized users.

Communicated by T.L. Grove

B. E. Mordick · A. F. Glazner (✉)
Department of Geological Sciences,
University of North Carolina,
Chapel Hill, NC 27599-3315, USA
E-mail: afg@unc.edu
Tel.: +1-832-6361393

Present address: B. E. Mordick
Anadarko Petroleum Corporation,
1201 Lake Robbins Drive, The Woodlands, TX 77380, USA
E-mail: briana_mordick@anadarko.com

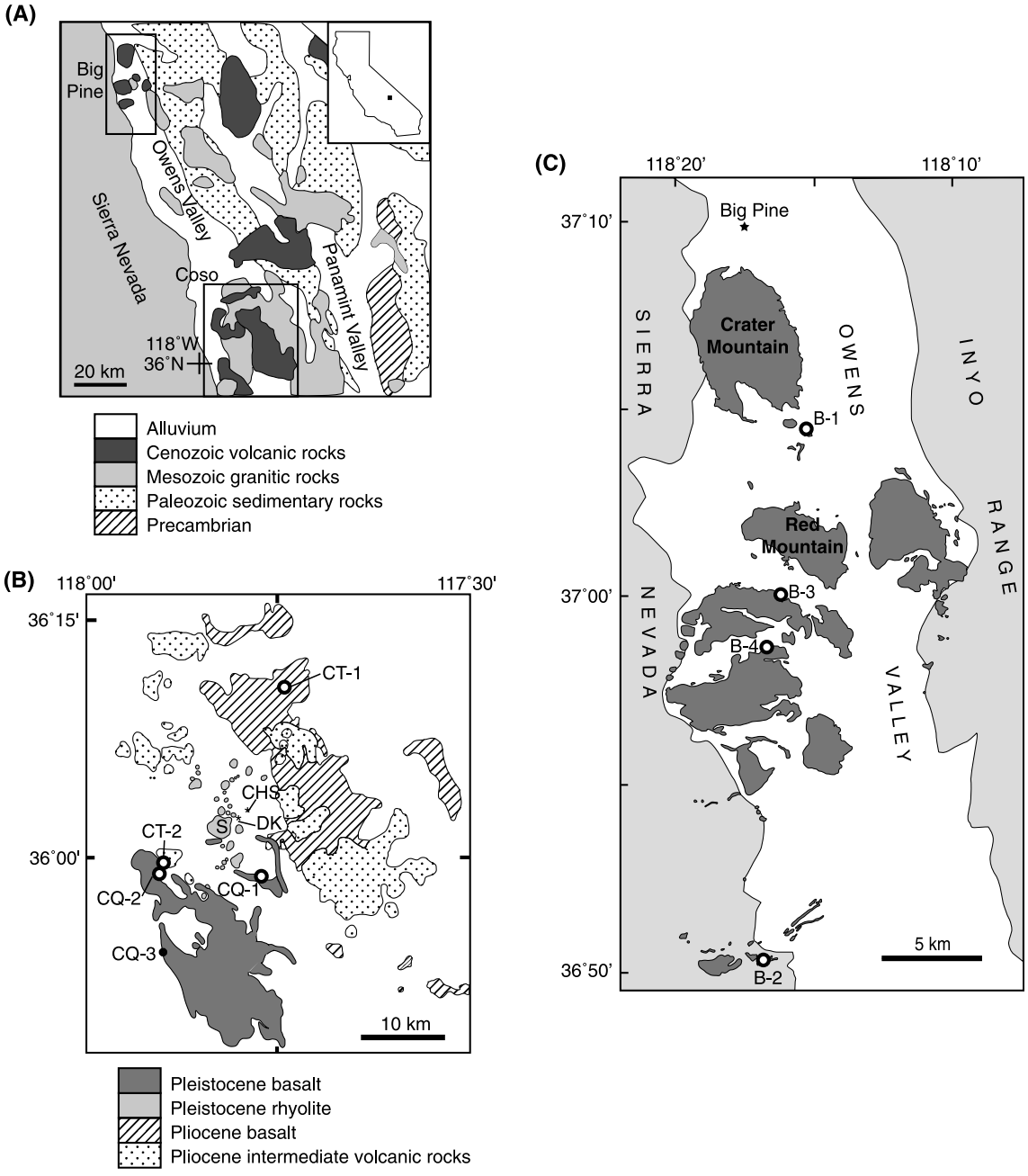

Fig. 1 **a** Location of Coso and Big Pine volcanic fields in eastern California, with samples locations marked. **b** Geologic map of the Coso volcanic field, modified from Novak and Bacon (1986). **c** Geologic map of the Big Pine volcanic field, modified from Moore (1963), Bateman (1965), Ross (1965), and Nelson (1966). *S* Sugarloaf Mountain, *DK* Devil's Kitchen, *CHS* Coso Hot Springs

sector), and how the presence of phenocrysts other than pyroxene affect calculated temperatures and pressures.

Background and previous work

Coso volcanic field

The Coso volcanic field is located in east-central California along the eastern front of the Sierra Nevada (Fig. 1). Volcanic rocks rest on a basement complex of Mesozoic plutonic and metamorphic rocks (Duffield et al. 1980; Bacon et al. 1984; Walker et al. 2002). There were two episodes of Cenozoic volcanism at Coso: one during the Pliocene, 4–2.5 m.y. ago, and one during the Pleistocene, 1.1–0.04 m.y. ago (Duffield et al. 1980; Bacon 1982; Bacon and Metz 1984). The Pliocene part of the field includes a full suite of volcanic rocks ranging from basalt to rhyolite and was by far the most voluminous, resulting in $\sim$ 30 km^3 of erupted material. During the Pleistocene only $\sim$ 5 km^3 of magma was erupted (Novak and Bacon 1986). The Pleistocene part

of the field is bimodal and consists of basaltic cinder cones and flows, high-silica rhyolite domes, and associated pyroclastic material. Several of these rhyolite domes contain andesitic enclaves (Duffield et al. 1980; Bacon 1982; Bacon and Metz 1984).

Pleistocene silicic magmas were most likely derived from partial melting or differentiation of mantle basalts (Bacon et al. 1981, 1984; Miller 1999; Manley and Bacon 2000; Miller and Wooden 2004). Trace element signatures suggest crystal fractionation from the parent basalt or intermediate magmas combined with assimilation of minor amounts of crustal material. These silicic reservoirs may be sustained by heat from basaltic magma (Bacon et al. 1981; Manley and Bacon 2000). Intrusion of basalt into the crust is facilitated by extension (Duffield et al. 1980; Bacon 1982; Bacon et al. 1984; Bacon and Metz 1984; Monastero et al. 2005). Petrographic evidence suggests that mixing and mingling occurred between basalt and rhyolite during the Pleistocene episode of volcanism (Bacon 1982; Bacon and Metz 1984).

The depth to the top of the rhyolite magma reservoir was estimated by Manley and Bacon (2000) to have risen from approximately 10 km 1 m.y. ago to approximately 5.5 km 0.1 m.y. ago. These depths were calculated from phenocryst compositions using the two-oxide thermometer and the Al-in-hornblende barometer (Manley and Bacon 2000).

Teleseismic P-wave tomography and receiver function studies suggest the presence of a low velocity body at a depth of 5–15 km, centered south of Coso Hot Springs (Fig. 1b; Reasenberg et al. 1980; Wilson et al. 2003). This zone is interpreted as a region of partial melt and is consistent with the presence of a system of mafic dikes oriented N–S below the rhyolite field (Duffield et al. 1980; Reasenberg et al. 1980; Bacon 1982; Bacon et al. 1984; Wilson et al. 2003). A region of anomalously high heat flow at Coso is also centered around Devil's Kitchen and Sugarloaf Mountain (Fig. 1b) and is consistent with the presence of a magma body at 5–20 km depth (Combs 1980). Gravity data also suggest the presence of a magma body under the rhyolite field (Plouff and Isherwood 1980; Wilson et al. 2003).

Big Pine volcanic field

The Big Pine volcanic field is also located along the eastern Sierran front in Owens Valley approximately 120 km north of the Coso volcanic field (Fig. 1). It consists of ~ 0.5 km^3 of Quaternary basalt erupted from $\sim$ 40 vents (Darrow 1972; Bierman et al. 1991; Beard and Glazner 1995; Fig. 1c). Most flows range in age from $\sim$ 0.1 to 0.5 m.y. and erupted from vents located on or near normal faults (Bierman et al. 1991). Mesozoic rocks of the Sierra Nevada batholith lie to the west and late Proterozoic and Paleozoic metasedimentary and Mesozoic metavolcanic rocks lie to the east (Beard and Glazner 1995). Sr isotopic studies place the Big Pine field on the North American craton and the Coso field on transitional or accreted lithosphere (Ormerod et al. 1988; Glazner and Miller 1997).

The tectonic setting of the Big Pine field changed from subduction of the Farallon plate before about 5 Ma to strike-slip associated with the developing San Andreas fault in the late Pliocene (Ormerod et al. 1991). The subduction setting produced basalts with chemical signatures from both the downgoing lithospheric slab enriched by subduction-related processes, and the asthenosphere underlying the overriding plate (Ormerod et al. 1988). Although the silica content of magmas increased over time in the Big Pine field, the chemical compositions of the magmas vary widely and reflect a range of magmatic processes including crystal fractionation, crustal assimilation, and reactions with mantle peridotite (Ormerod et al. 1991). Basalts from the Big Pine field are among the most primitive in the Basin and Range (Wang et al. 2002), and the presence of mantle xenoliths suggests rapid ascent of magmas from mantle depths.

Methods

Sampling strategy

Sampling strategy focused on collecting fresh rocks with visible pyroxene phenocrysts. Because the thermobarometer requires that the whole-rock and pyroxene compositions be in equilibrium with one another, an ideal sample is one in which the only phenocrysts present are sparse pyroxene crystals. However, none of the samples fit this strict criterion. The Coso volcanic field consists of at least 13 Pleistocene and 5 Pliocene basalt flows (Duffield and Bacon 1980). The Big Pine volcanic field consists of at least 30 Quaternary basalt flows (Moore 1963; Bateman 1965; Ross 1965; Nelson 1966). Those flows that were previously described as containing pyroxene phenocrysts were targeted for sampling.

Analytical methods

Whole-rock analyses were performed using the direct-current plasma (DCP) spectrometer at UNC-CH. Samples were prepared for analysis following the procedure of Beard and Glazner (1995) and were analyzed in duplicate.

All microprobe analyses were performed on the Cameca Camebax electron microprobe at Duke University. Analyses were performed at 15 kV and a sample current of 15 nA. Where possible, several pyroxene grains within one sample were analyzed. Within each grain multiple analyses were taken to account for the differences between core and rim composition and/or sector zoning. The electron beam is $\sim 2-4$ μm in diameter. At each location sampled within one grain, two points were analyzed no more than several beam widths from each

other to account for variations arising from machine conditions; hypothetically, composition should not vary significantly over such a small distance. Each pyroxene grain was analyzed at no fewer than ten spots (giving at least ten separate chemical analyses) on at least two different days.

Thermobarometric calculations

The clinopyroxene thermobarometer was developed by Putirka et al. (1996) and uses the compositions of clinopyroxene and coexisting liquid to determine the temperature and pressure at which these two phases were last in equilibrium. The thermobarometer is based on the following equilibria:

$$2SiO_2^{liq} + NaO_{1/2}^{liq} + AlO_{3/2}^{liq} = NaAlSi_2O_6^{px}(Jd) \quad (1)$$

$$CaFmSi_2O_6^{px}(Di) + NaO_{1/2}^{liq} + AlO_{3/2}^{liq} = NaAlSi_2O_6^{px}(Jd) + CaO^{liq} + FmO^{liq} \quad (2)$$

where Jd and Di are jadeite and diopside molecules. Quantities such as "Ca^{liq}" are the cation fraction of the given oxide in the liquid, the mole fractions of the pyroxene components (e.g., Jd^{px}) are calculated according to a normative scheme, and Fm = FeO + MgO (Putirka et al. 1996). FeO in the liquid is set as $0.9\times Fe_2O_3$. In addition to the cation assignment procedure outlined in Putirka et al. (1996), the following equations were also used for the pyroxene calculation:

$$Fe^{3+} = Na + Al^{IV} - Al^{VI} - 2Ti - Cr \quad (3)$$

$$Fe^{2+} = Fe - Fe^{3+} \quad (4)$$

with cations calculated per six oxygens (K. Putirka, personal communication).

All of these quantities can be calculated from chemical analyses of the magmatic liquid and pyroxene crystals. Both reactions (1 and 2) are sensitive to pressure and temperature and, in combination with fundamental thermodynamic equations, Putirka et al. (1996) derived the following equations for the temperature and pressure of pyroxene crystallization:

$$P(\text{MPa}) = -5,430 + 2.99T(\text{K}) + 0.364T(\text{K})\ \ln\left[\frac{Jd^{px}}{[Si^{liq}]^2 \times Na^{liq} \times Al^{liq}}\right] - 36,700\left[Na^{liq} \times Al^{liq}\right] \quad (5)$$

$$\frac{10^4}{T(\text{K})} = 6.73 - 0.26 \times \ln\left[\frac{Jd^{px} \times Ca^{liq} \times Fm^{liq}}{DiHd^{px} \times Na^{liq} \times Al^{liq}}\right] - 0.86 \times \ln\left[\frac{Mg^{liq}}{Mg^{liq} + Fe^{liq}}\right] + 0.52 \times \ln[Ca^{liq}] \quad (6)$$

Equation 3 estimates pressures to ±140 MPa and Eq. 4 estimates temperatures to ±27 K (Putirka et al. 1996). Equations 3 and 4 can be represented as curves on a pressure vs. temperature graph (inset, Fig. 3a). The place where the two curves cross represents a unique pressure and temperature solution for the mineral–liquid pair. Pressure is converted to depth by assuming an average crustal thickness of 33 km (Jones et al. 1992; Ruppert et al. 1998; Wang et al. 2002), an average crustal density of 2,750 kg/m^3, and an average mantle density of 3,250 kg/m^3 (Jones et al. 1992; Fliedner et al. 1996; Wang et al. 2002).

Results

Petrography

All samples are nepheline-normative alkali olivine basalts except one sample from the Big Pine field, B-2, which is a hypersthene-normative olivine tholeiite. The primary phenocryst phases are olivine, plagioclase, and clinopyroxene. The groundmass typically consists of brownish-black glass, olivine, plagioclase, clinopyroxene, and opaque minerals. Phenocryst contents vary from 5 to 29 vol% with the majority of phenocrysts being smaller than 2 mm. The abundance of vesicles varies from 0 to 14 vol% (eTable 1).

The whole-rock composition used for calculating temperature and pressure must reflect the composition of liquid in equilibrium with pyroxene in order for the correct temperatures and pressures to be calculated. Because other phenocryst phases are present in the samples, the bulk whole-rock compositions may therefore not be appropriate for the calculations and corrections for phenocryst content must be made. To make this correction the proportion of phenocrysts in each sample was calculated by point counting (eTable 1). Five hundred points were counted for each thin section two separate times and the values averaged. All point counting was performed at 100× magnification.

The distinction between groundmass and phenocryst was determined visually and varied from sample to sample. This distinction was based on the appearance of homogeneity. Because most basalts display intersertal texture, at high enough magnification all the phases that make up the "groundmass" should be identifiable as individual minerals or glass, making the distinction between groundmass and phenocrysts subjective. By performing point counting only at 100× magnification, groundmass was designated as appearing to be a homogeneous black/brown mass whereas phenocrysts were anything that appeared distinct from this homogeneous mass. For some samples, this meant that a phenocryst could be something as small as a tenth of a millimeter.

Samples with ≤ 10 vol% phenocrysts were not corrected for the effect of phenocrysts on equilibrium inasmuch as removing the contribution of small volumes of crystals does not significantly change the whole-rock chemical composition. Corrections were made by first converting vol% phenocrysts to wt% phenocrysts and

then subtracting the entire wt% olivine, the entire wt% plagioclase, and the combined wt% of both olivine and plagioclase (eTables 1, 2). Each of these corrected compositions was then used to calculate the temperatures and pressures of pyroxene crystallization.

Geochemistry

Analytical data are presented in Tables 1 and 2 and eTables 3 and 4 . Reported precisions are the standard deviation of the mean (standard error), s.e. $= s/\sqrt{n}$, where s.e. is standard error, s is the standard deviation of the mean of each set of analyses for each sample, and n is the number of analyses of each sample.

Whole-rock chemical analyses are presented in Table 1. Each sample was prepared in two separate batches and analyzed four times during each DCP run. Those samples for which poor analyses were obtained (i.e., low or high totals) were run a second time using the same sample preparation.

Chemical data are for pyroxene phenocrysts are presented in Table 2 and olivine and plagioclase chemical data are presented in eTable 3. The average composition of Coso pyroxene expressed as end members wollastonite (Wo), enstatite (En), and ferrosilite (Fs) is $Wo_{46}En_{44}Fs_{11}$, with ranges $Wo_{42\text{-}48}$, $En_{39\text{-}48}$, and $Fs_{7\text{-}13}$. The average Coso olivine composition is Fo_{83} ($Fo_{80\text{-}87}$) and the average Coso plagioclase composition is An_{79} ($An_{76\text{–}81}$). The average composition of Big Pine pyroxene is $Wo_{44}En_{46}Fs_{9}$ ($Wo_{42\text{-}47}$, $En_{42\text{-}50}$, $Fs_{6\text{-}11}$). The average Big Pine olivine composition is Fo_{89} ($Fo_{88\text{-}91}$) and the average Big Pine plagioclase composition is An_{86} ($An_{85\text{-}86}$). Analytical data for zoned pyroxenes are presented in eTable 4.

Thermobarometry

Calculated temperatures and pressures for nine samples are presented in Table 3 and Fig. 2. The average temperature and pressure of pyroxene crystallization are 1,301°C and 1,440 MPa for the Big Pine basalts, 1,183°C and 530 MPa for Pliocene Coso basalts, and 1,223°C and 900 MPa for Pleistocene Coso basalts.

Several temperatures and pressures were calculated for each sample by using the average composition of each pyroxene grain in a sample (Table 2) paired with the whole-rock composition. Temperatures and pressures were calculated using Eqs. 5 and 6. If a grain was significantly zoned then calculations were also made using the average compositions of the zones. The sample average in Table 3 is the average of these grain average temperatures and pressures for each sample except for sector-zoned sample CT-2, where the sample average used only the pyroxene sectors deemed to be in equilibrium with the liquid (see discussion of sector zoning below). Grand mean temperatures and pressures for each volcanic field were calculated by averaging the sample average temperatures and pressures for each sample from each field.

Discussion

Errors in input data: Monte Carlo analysis

The pressures calculated using the pyroxene thermobarometer are sensitive to temperature. Even a slight change in the calculated temperature can lead to a significant change in the calculated pressure (inset, Fig. 3a);

Table 1 Whole rock major element chemical data

Field	Coso										Big Pine							
Sample Field name	CT-1 CP524-02		CQ-1 CW525-01		CQ-2 RH523-01		CT-2 RV524-01		CQ-3 SLL524-06		B-1 FS526-01		B-2 OC526-01		B-3 TC526-01		B-4 WA526-01	
SiO_2	50.42	*0.47*	48.28	*0.30*	50.19	*0.28*	52.27	*0.66*	52.25	*0.53*	52.91	*0.48*	46.26	*0.35*	47.41	*0.32*	49.08	*0.45*
TiO_2	1.28	*0.05*	1.94	*0.04*	1.43	*0.04*	1.72	*0.06*	1.71	*0.05*	1.40	*0.03*	1.82	*0.04*	1.32	*0.03*	1.40	*0.03*
Al_2O_3	17.10	*0.31*	17.03	*0.27*	17.61	*0.38*	17.36	*0.26*	16.66	*0.35*	16.99	*0.35*	15.33	*0.26*	13.51	*0.36*	15.89	*0.29*
$Fe_2O_3^t$	8.56	*0.14*	10.22	*0.14*	8.88	*0.15*	8.55	*0.10*	8.92	*0.19*	7.22	*0.11*	10.19	*0.15*	8.89	*0.15*	9.04	*0.16*
MnO	0.15	*0.01*	0.16	*0.01*	0.15	*0.01*	0.14	*0.01*	0.15	*0.01*	0.11	*0.00*	0.16	*0.00*	0.15	*0.00*	0.16	*0.01*
MgO	7.04	*0.27*	7.11	*0.10*	7.15	*0.25*	4.69	*0.18*	5.57	*0.19*	6.35	*0.19*	10.15	*0.25*	12.93	*0.39*	9.64	*0.27*
CaO	11.04	*0.42*	9.72	*0.14*	10.38	*0.37*	8.04	*0.36*	8.63	*0.34*	8.51	*0.27*	10.79	*0.24*	11.62	*0.37*	10.50	*0.31*
Na_2O	3.48	*0.16*	3.60	*0.07*	3.51	*0.13*	4.27	*0.11*	3.95	*0.11*	3.49	*0.08*	3.50	*0.18*	2.75	*0.13*	3.06	*0.11*
K_2O	1.21	*0.05*	1.33	*0.04*	1.19	*0.05*	2.25	*0.05*	1.79	*0.05*	2.49	*0.05*	1.47	*0.04*	1.31	*0.02*	1.79	*0.09*
Ba	1,104	*35*	462	*8*	734	*34*	717	*28*	898	*32*	1,477	*34*	1,415	*22*	1,283	*29*	1,604	*32*
Sr	1,032	*30*	739	*10*	1,052	*28*	784	*18*	669	*16*	1,211	*23*	1,925	*25*	1,370	*31*	1,645	*31*
Total	100.29		99.39		100.47		99.29		99.62		99.47		99.67		99.87		100.56	
LOI	0.23		0.00		0.21		0.11		0.55		0.71		0.10		0.72		0.22	
n	10		10		12		12		10		11		6		8		11	
Map unit	Tbc		Qbc		Qbr		Tbr		Qbl		Qyb		QTbo		Qyb		Qba	
Age (my)	3.6 ± 0.1		1.1 ± 0.1		0.14 ± 0.09		2.1 ± 0.3		0.40 ± 0.05		0.31 ± 0.04		0.09–1.18		0.13 ± 0.09		0.13 ± 0.09	
N Lat.	36.1872		35.9789		35.9728		36.0010		35.9079		37.0712		36.8463		37.0661		36.9812	
W Long.	117.7150		117.7714		117.9101		117.9008		117.8904		118.2550		118.2862		118.2619		118.2829	

One standard deviation of the mean in italics. Map unit designations from Moore (1963) and Bateman (1964)
LOI loss on ignition

Table 2 Compositions of unzoned pyroxene crystals

Field	Sample	Grain	SiO_2	TiO_2	Al_2O_3	FeO	MnO	MgO	CaO	Na_2O	Cr_2O_3	Total	*n*
Coso	CT-1	1a	50.25	0.58	4.79	4.64	0.02	15.70	23.52	0.31	0.57	100.37	33
			0.76	*0.10*	*0.57*	*0.26*	*0.04*	*0.38*	*0.73*	*0.03*	*0.25*		
		1b	50.29	0.56	4.85	4.65	0.03	15.63	23.17	0.31	0.61	100.10	35
			0.63	*0.09*	*0.49*	*0.24*	*0.04*	*0.32*	*0.72*	*0.04*	*0.31*		
		1c	50.19	0.52	5.06	4.54	0.07	15.56	22.56	0.34	0.77	99.61	14
			0.34	*0.07*	*0.16*	*0.19*	*0.05*	*0.25*	*0.55*	*0.03*	*0.30*		
		2	51.16	0.45	4.03	4.66	0.10	16.15	22.10	0.29	0.37	99.31	10
			1.13	*0.17*	*1.04*	*0.30*	*0.03*	*0.65*	*0.19*	*0.03*	*0.20*		
		3	48.90	0.50	4.59	4.64	NA	16.04	23.52	0.32	0.53	99.05	10
			0.63	*0.09*	*0.74*	*0.18*		*0.56*	*0.30*	*0.02*	*0.13*		
	CQ-1	1	49.40	0.84	6.33	6.45	0.13	15.09	20.66	0.61	0.10	99.62	20
			0.31	*0.07*	*0.28*	*0.14*	*0.03*	*0.27*	*0.18*	*0.03*	*0.06*		
	CQ-2	1	48.75	1.01	5.04	7.25	NA	14.99	22.43	0.43	0.18	100.07	40
			1.13	*0.25*	*1.14*	*1.20*		*0.65*	*0.56*	*0.05*	*0.14*		
		2	50.09	0.74	5.01	7.11	0.14	15.25	20.84	0.45	0.09	99.72	31
			0.55	*0.12*	*0.93*	*1.36*	*0.04*	*0.43*	*0.64*	*0.04*	*0.10*		
	CT-2	1	50.95	0.95	2.86	7.67	0.19	14.92	21.67	0.38	0.02	99.60	12
			0.35	*0.10*	*0.20*	*0.16*	*0.02*	*0.18*	*0.19*	*0.02*	*0.03*		
		2	49.21	1.21	3.91	7.82	NA	14.50	22.62	0.40	0.04	99.71	28
			1.45	*0.45*	*1.35*	*0.44*		*0.86*	*0.31*	*0.06*	*0.03*		
		3	49.19	1.24	4.07	7.82	0.20	14.61	22.41	0.42	0.03	99.84	39
			1.87	*0.43*	*1.53*	*0.32*	*0.03*	*0.86*	*0.92*	*0.05*	*0.03*		
	CQ-3	1	49.48	0.82	5.12	7.58	0.16	15.47	20.00	0.57	0.29	99.47	21
			0.59	*0.13*	*0.69*	*0.62*	*0.03*	*0.52*	*0.44*	*0.03*	*0.10*		
		2	51.01	0.57	5.34	5.71	0.13	16.49	20.36	0.49	0.27	100.36	19
			0.60	*0.12*	*0.27*	*0.31*	*0.02*	*0.44*	*0.23*	*0.04*	*0.21*		
Big Pine	B-1	1	51.65	0.35	5.39	4.67	0.09	17.25	20.19	0.50	0.19	100.29	38
			0.68	*0.06*	*0.69*	*0.17*	*0.03*	*0.31*	*0.40*	*0.03*	*0.13*		
		2	48.36	1.01	7.83	5.82	0.10	14.97	20.77	0.62	0.01	99.50	24
			0.74	*0.21*	*0.64*	*0.19*	*0.02*	*0.49*	*0.39*	*0.05*	*0.02*		
	B-2	1	49.47	0.51	7.19	5.98	0.13	14.94	20.26	0.86	0.53	99.87	24
			0.52	*0.09*	*0.52*	*0.61*	*0.03*	*1.46*	*1.87*	*0.11*	*0.11*		
	B-3	1	49.20	0.69	7.65	6.00	0.11	15.13	21.01	0.65	0.07	100.45	33
			0.84	*0.13*	*0.84*	*0.35*	*0.03*	*0.56*	*0.47*	*0.05*	*0.04*		
		2	51.73	0.32	4.18	3.99	0.08	17.38	21.74	0.48	0.43	100.15	43
			0.80	*0.08*	*0.54*	*0.20*	*0.03*	*0.37*	*0.65*	*0.03*	*0.11*		
		3	47.14	1.29	8.28	6.90	0.14	13.84	21.41	0.66	0.11	99.76	25
			1.03	*0.36*	*1.19*	*0.68*	*0.03*	*0.56*	*0.97*	*0.14*	*0.19*		
	B-4	1	48.87	0.49	8.03	5.14	0.12	15.66	21.15	0.55	0.17	100.09	34
			0.66	*0.06*	*0.58*	*0.18*	*0.03*	*0.30*	*0.37*	*0.04*	*0.05*		
		2	49.12	0.54	7.74	6.62	0.14	15.35	19.58	0.72	0.03	99.80	25
			0.99	*0.12*	*1.12*	*0.39*	*0.03*	*0.82*	*0.41*	*0.08*	*0.02*		

One standard deviation of the mean in italics
NA not analyzed

thus, analytical error will cause calculated P and T to covary in the absence of any real variation in P and T. Such a trend could easily be mistaken for a local geothermal or adiabatic gradient.

In order to determine the potential significance of these problems, a Monte Carlo analysis was performed following the method of Steltenpohl and Bartley (1987). Pyroxene and liquid chemical data of sample CQ-2 were chosen as a test sample. Two hundred normally distributed random numbers were generated for each oxide using the CQ-2 grain 1 pyroxene chemical composition and standard error values and the CQ-2 whole-rock chemical composition and standard error values (Tables 1, 2, respectively). These values were then paired and Eqs. 5 and 6 were used to calculate temperature and pressure. The resulting temperatures and pressures are plotted in Fig. 3a, b.

The trend observed in these fictive results mimics the peridotite solidus or adiabatic gradient (Takahashi and Kushiro 1983; McKenzie and Bickle 1988), but it is actually a result of interdependence of the P–T equations and does not describe P–T variation beneath the volcanic field (Fig. 3a, b). One must be careful not to assign any meaningful interpretation to this trend.

Using the values generated by the Monte Carlo analysis the resulting mean T and P for sample CQ-2 are $1{,}218 \pm 3$°C and 810 ± 40 MPa. The actual T and P values calculated for sample CQ-2, grain 1 are similar: 1,219°C and 830 MPa. Furthermore, the dispersion of the Monte Carlo values is low and well within model and analytical error. This result indicates that as long as analytical error is low, temperatures and pressures calculated using the thermobarometer will be both precise and accurate.

Table 3 Temperatures and pressures of pyroxene crystallization

Field	Age	Sample	Grain	Pyroxene description	*T* (°C)	*P* (MPa)	*D* (km)
Coso	Pliocene	CT-1		Sample average	1,196	550	15.1
			1	Zone A	1,194	540	14.7
			1	Zone B	1,197	550	15.3
			1	Zone C	1,203	620	17.1
			1	Grain average	1,197	560	15.4
			2	Grain average	1,195	510	14.2
			2	Zone A	1,197	580	16.0
			2	Zone B	1,197	580	15.9
			2	Grain average	1,197	580	15.9
		CT-2		Sample average	1,170	510	14.0
			1	Grain average	1,168	490	13.4
			2	A sector	1,165	450	12.4
			2	B sector	1,116	−190	−5.2
			2	Grain average	1,147	220	6.0
			3	A sector	1,176	590	16.3
			3	B sector	1,137	70	1.9
			3	Grain average	1,152	270	7.5
	Pleistocene	CQ-1		Sample average	1,241	1,120	30.9
		CQ-2		Sample average	1,223	850	23.5
			1	Grain average	1,219	830	22.8
			2	Zone A	1,226	880	24.1
			2	Zone B	1,226	880	24.3
			2	Grain average	1,226	880	24.2
		CQ-3		Sample average	1,215	840	23.2
			1	Grain average	1,219	910	25.0
			2	Grain average	1,210	780	21.5
Pliocene average					1,183	530	14.6
Pleistocene average					1,223	900	24.9
Coso average					1,201	700	19.3
Big Pine	Pleistocene	B-1		Sample average	1,253	1,020	28.1
			1	Core	1,247	950	26.0
			1	Rim	1,240	880	24.1
			1	Grain average	1,245	930	25.6
			2	Grain average	1,260	1,120	30.7
		B-2		Sample average	1,308	1,680	54.6
		B-3		Sample average	1,332	1,640	53.4
			1	Core	1,345	1,780	57.8
			1	Rim	1,339	1,710	55.5
			1	Grain average	1,341	1,730	56.4
			2	Zone A	1,311	1,430	46.4
			2	Zone B	1,312	1,430	46.6
			2	Zone C	1,313	1,420	46.1
			2	Grain average	1,312	1,430	46.4
			3	Core	1,356	1,910	62.0
			3	Rim	1,315	1,470	47.7
			3	Grain average	1,343	1,770	57.4
		B-4		Sample average	1,299	1,420	46.3
			1	Core	1,288	1,300	42.3
			1	Rim	1,286	1,280	41.6
			1	Grain average	1,287	1,290	42.0
			2	Grain average	1,311	1,550	50.5
Big Pine average					1,301	1,440	45.4

Determination of equilibrium compositions

The thermobarometer requires input of a pyroxene chemical composition and the composition of the liquid with which it is in equilibrium. Extreme non-equilibrium is easily recognized as it leads to calculation of erroneous temperatures and pressures (i.e., significantly negative values) but it is not readily apparent whether near-equilibrium discrepancies will significantly affect the calculation. Possible problems in determining the equilibrium chemical composition include the presence of sector and/or core-to-rim zoned pyroxene crystals and the presence of other phenocrysts.

Sector zoning

One sample in this study contained pyroxene phenocrysts that were consistently sector zoned: sample CT-2, a Pliocene basalt from the Coso field. Ordinarily,

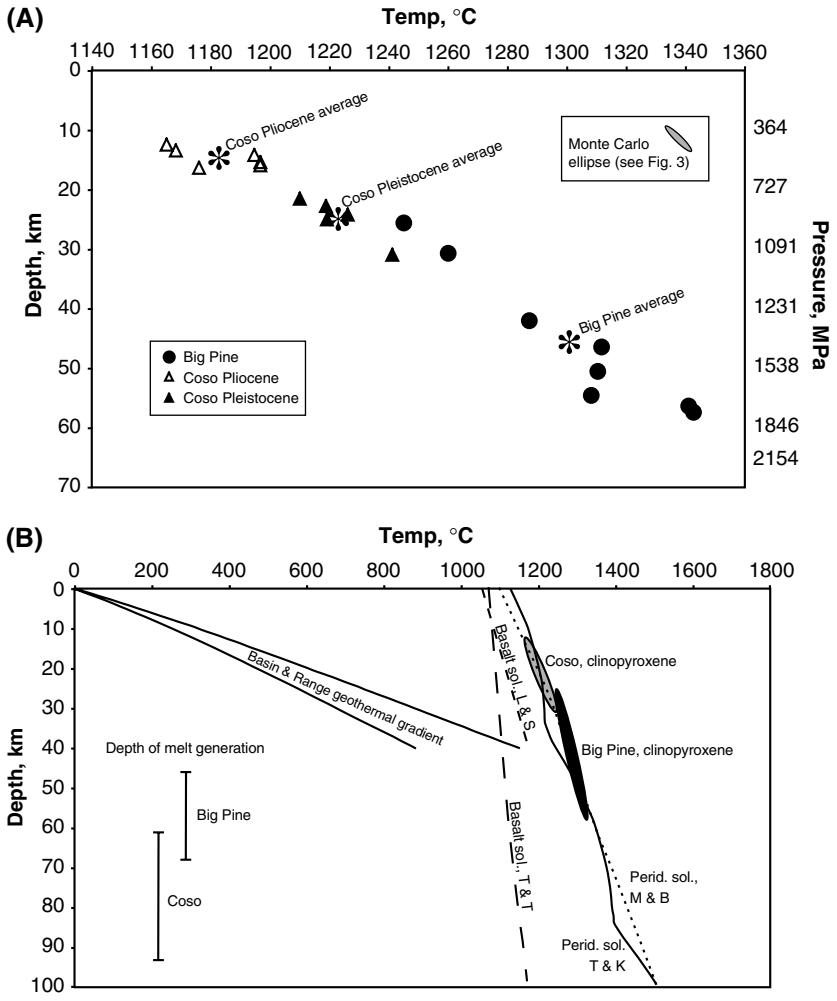

Fig. 2 **a** Temperatures and pressures of pyroxene crystallization. Values plotted are "grain averages" from each sample in each field unless only one grain was analyzed, in which case the value plotted is the "sample average" (Table 3). *Inset*: approximate size of Monte Carlo error ellipse (Fig. 3). **b** Summary of temperature and pressure values as above. Also plotted are the depth of melt generation at Big Pine and Coso from Wang et al. (2002)—values have no temperature significance, the characteristic Basin and Range geothermal gradient envelope and basalt solidus of Lachenbruch and Sass (1978), the peridotite solidi of McKenzie and Bickle (1988) and Takahashi and Kushiro (1983), and the basalt solidus of Tsuruta and Takahashi (1998)

determination of crystallographic faces is required to hypothesize which sectors may be out of equilibrium according to the criteria of Nakamura (1973). However, because the thermobarometer has a low tolerance for non-equilibrium pyroxene–liquid pairs, the non-equilibrium faces are apparent from calculated temperatures and pressures for each zone.

In each of the two sector-zoned pyroxenes analyzed from sample CT-2, the chemical composition of one sector resulted in the calculation of negative or unreasonably low pressures (the B sectors of both grains) whereas the chemical composition of the other sector (the A sectors of both grains) gave pressures and temperatures similar to the other samples from the Coso field (Table 3). In addition, one non-sector-zoned pyroxene crystal from sample CT-2 was analyzed (grain 1), and the pressures and temperatures calculated for this grain were similar to the pressures and temperatures calculated for the A sectors of both sector-zoned grains. It is therefore reasonable to assume that these A sectors represent near-equilibrium crystallization conditions.

Core-to-rim zoning

Three samples of Quaternary basalts from the Big Pine field contain pyroxene grains with significant core-to-rim compositional variations: B-1, B-3, and B-4. The differences in composition between core and rim for samples B-1 and B-4 represent differences in temperature and pressure of crystallization of < 10°C and < 100 MPa, respectively. For sample B-3, two pyroxene grains (1 and 3) show core-to-rim zoning. The results for grain 1 are similar to those of samples B-1 and B-4, with only minor differences in calculated temperature and pressure that are within analytical and model error. For grain 3, however, the compositional differences between core and rim represent a difference in temperature of 41°C and in pressure of 440 MPa. These differences cannot be accounted for by analytical or model error and may represent differences in crystallization conditions between core and rim.

In all cases, the temperatures and pressures calculated for the rim are lower than those calculated for the core. Clearly, if the core and rim of a grain have different

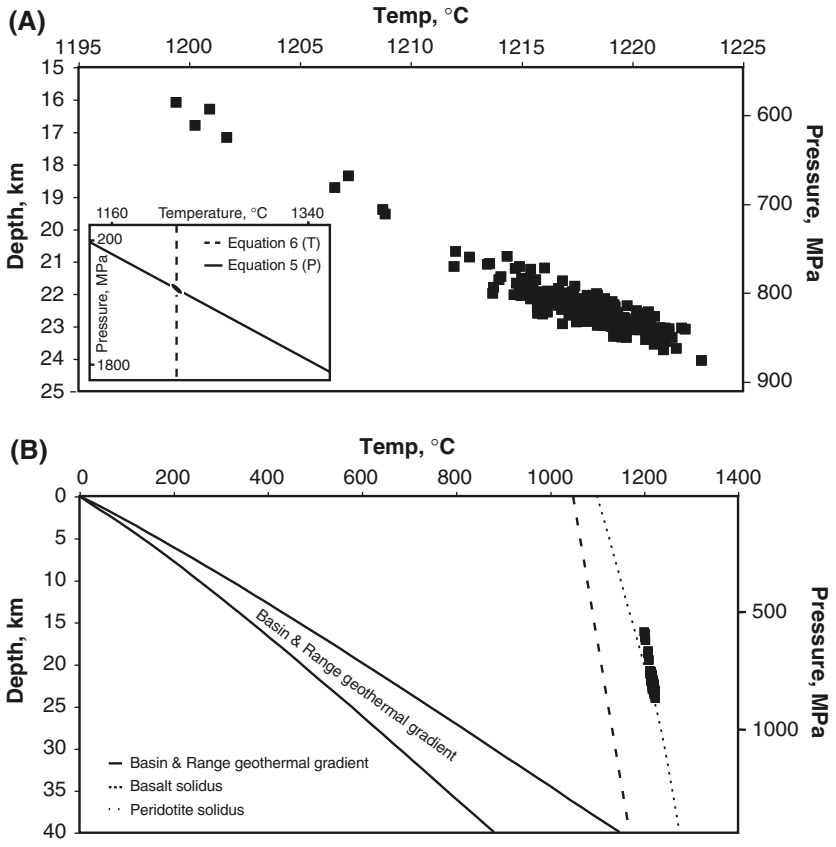

Fig. 3 **a** Results of the Monte Carlo analysis. The average T and P of the Monte Carlo analysis, 1,218 ± 3°C and 810 ± 40 MPa, differ insignificantly from the calculated T and P for sample CQ-2, 1,219°C and 830 MPa. The scatter at low temperature and pressure values is likely a result of non-equilibrium pyroxene–liquid pairs. *Inset*: graphical representation of the pressure and temperature equations, scaled to the area covered by Fig. 2a. The ellipse is the approximate error ellipse defined by the Monte Carlo temperatures and pressures in **a**. **b** Results of the Monte Carlo analysis plotted with the characteristic Basin and Range geothermal gradient envelope, basalt solidus of Lachenbruch and Sass (1978), and peridotite solidus of McKenzie and Bickle (1988)

chemical compositions then they cannot both be in equilibrium with the same liquid at comparable pressures and temperatures. It is possible that the differences in composition between rim and core record real changes in temperature and pressure as the magma rose from depth and pyroxene crystallized, but more analyses and consistency tests are necessary.

Correction for the presence of phenocrysts other than pyroxene

Because crystallization of phenocryst phases changes the composition of the liquid in equilibrium with the pyroxene, it is necessary to determine the effect this has on calculated temperature and pressure. Attempting to determine what combination of groundmass and phenocrysts represents the composition of liquid in equilibrium with pyroxene can lead to some dubious assumptions. To determine which phenocrysts were present when pyroxene was crystallizing an order of crystallization must be assumed. This is a difficult task when dealing with basalts because textural evidence is generally not conclusive (Marsh 1981). Furthermore, this can become extremely complex when trying to determine what percentage of phenocrysts likely crystallized before, during, and after pyroxene crystallization.

Sample CQ-2, a Pleistocene Coso basalt, was chosen as a test sample for these corrections because it contains a significant concentration of phenocrysts of olivine, plagioclase, and pyroxene, and because the pyroxene phenocrysts are slightly poikilitic with small inclusions of both olivine and plagioclase, indicating that these two phases had either crystallized before or simultaneously with pyroxene. Consequently, it was reasonable to assume that pyroxene was one of the last phases to crystallize, and that the composition of the liquid with which it was in equilibrium could be determined by subtracting the chemical compositions of both olivine and plagioclase from the whole-rock chemical composition. Sample CQ-2 contains 15 wt% plagioclase phenocrysts and 5 wt% olivine phenocrysts. When these contributions are removed from the whole-rock composition, the resulting calculated temperature of crystallization decreases by 26° and the pressure of crystallization decreases by 120 MPa (Fig. 4).

For all samples, removing plagioclase from the whole-rock composition increases the calculated temperature and pressure of pyroxene crystallization whereas removing olivine decreases the temperature and pressure (Fig. 4). This is largely a result of olivine removal driving up, and plagioclase removal driving down, the concentration of Na in the liquid. Additionally, removing olivine from the whole rock produces a greater change in temperature and pressure than removing an equal mass of plagioclase. In the case of

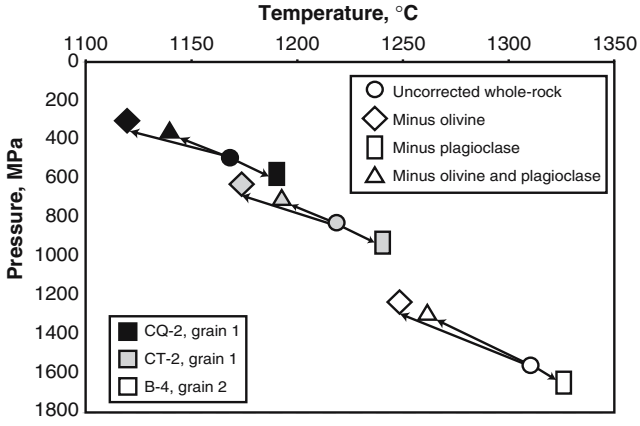

Fig. 4 Variation of temperature and pressure of pyroxene crystallization with whole-rock chemical composition. Removing olivine from the whole-rock composition (*diamonds*) decreases the calculated temperature and pressure of pyroxene crystallization. Removing plagioclase (*rectangles*) increases the calculated temperature and pressure of pyroxene crystallization. In most cases, removing both olivine and plagioclase from the whole-rock composition (*triangles*) decreases the calculated temperature and pressure of crystallization because removing olivine results in a larger change in calculated temperature and pressure than removing an equal amount of plagioclase. See Table 4 for complete temperature and pressure data

CQ-2, removing 15 wt% plagioclase increases the calculated T and P $\sim$ 22°C and $\sim$ 100 MPa whereas removing 5 wt% olivine decreases the calculated T and P by $\sim$ 45°C and $\sim$ 200 MPa. Because the differences in calculated temperature and pressure in all three cases (removing ol + plag, plag only, and olivine only) are within model and analytical error it is reasonable to assume that correcting for the presence of other phenocrysts produces only a small change in temperature and pressure for samples with sparse phenocrysts.

Similar calculations were performed on all other samples where the volume of phenocrysts is greater than 10% (Table 4 , eTable 2). For all but sample B-3, a Pleistocene Big Pine basalt, the above assumption is reasonable. This sample contains 4 wt% plagioclase phenocrysts and 23 wt% olivine phenocrysts. Subtracting these from the whole-rock composition decreases the temperature of pyroxene crystallization of grain 1 by $\sim$ 255°C and the pressure by $\sim$ 1,250 MPa. This is well outside estimated error of the thermobarometer. However, subtracting the entire contributions of olivine and plagioclase is an unreasonable assumption. The majority of pyroxene grains in this sample are euhedral to subhedral and contain no inclusions of olivine or pyroxene. Also, the majority (14 vol%) of olivine phenocrysts and all plagioclase phenocrysts are small ($<$2 mm) suggesting that they potentially crystallized late. This would indicate that pyroxene was one of the first phases to crystallize and therefore removing the contributions of the plagioclase and olivine from the whole-rock composition would result in the calculation of inaccurate temperatures and pressures. Furthermore, the temperatures and pressures calculated for this sample, without correcting the whole rock for equilibrium, are similar to those obtained for other samples from the Big Pine field, suggesting that the uncorrected whole-rock composition is a better representative of the liquid than the corrected composition.

For most samples, it is probably reasonable to assume that some crystallization of other phenocrysts had occurred prior to the crystallization of pyroxene, and therefore minor adjustments should be made to the whole-rock composition. Precisely determining how large a contribution there is from other phenocrysts relies on too many assumptions to be done reasonably. As noted earlier, removing only small amounts of olivine and plagioclase from the whole-rock composition has a small effect on the calculated temperatures and pressures of pyroxene crystallization, and in most cases the differences are within analytical and model error. For the purposes of this study, it is reasonable to assume that the uncorrected whole-rock chemical composition is an accurate representation of the liquid that was in equilibrium with the pyroxene. Consequently, the temperatures and pressures of pyroxene crystallization discussed for each sample will be those calculated from the uncorrected whole-rock data.

The obstacles in determining equilibrium chemical compositions are not insurmountable. If possible, it is best to avoid sector and core-to-rim zoned grains and to choose samples that contain a small volume percent phenocrysts. When this is not possible one must determine whether these corrections, and the additional error incurred by making them, are necessary.

Comparison to previous work

Clinopyroxene thermobarometry indicates that the average crystallization depth of Coso basalts is $\sim$ 19 km whereas the average crystallization depth of Big Pine basalts is $\sim$ 45 km (Table 3). Wang et al. (2002) used a geochemical technique borrowed from mid-ocean ridge petrology to estimate the depth of melt generation at Coso and Big Pine as 93–61 and 68–46 km, respectively (Figs. 2b, 5). If correct, their results require that clinopyroxene crystals in Big Pine basalts began crystallizing after little or no ascent from the depth of melt generation. Conversely, clinopyroxene crystals in Coso basalts did not begin crystallizing until magma had ascended a minimum of $\sim$ 40 km from the depth of melt generation, or began crystallizing deeper but stalled at shallower depths for an amount of time significant enough to allow the crystals to re-equilibrate. These observations are consistent with the hypotheses that Big Pine basalts erupted directly from asthenospheric depth whereas Coso basalts first stalled in the crust, providing the heat source for the generation of rhyolitic melt.

Ducea and Saleeby (1996) determined the temperatures and pressures of crystallization of mantle xenoliths from the eastern Sierra Nevada region—the same mantle xenoliths found in the Big Pine basalts—and found that pressures range from approximately 1 to 2 GPa. The

Table 4 Temperatures and pressures of pyroxene crystallization calculated using whole-rock chemical compositions corrected for the presence of phenocrysts other than pyroxene

Field	Sample	Grain	Pyroxene description	Phenocryst correction	*T* (°C)	*P* (MPa)	*D* (km)
Big Pine	B-2		Sample average	9% ol	1,239	1,330	43.3
	B-3	1	Grain average	4% plag, 23% ol	1,086	480	13.2
		1	Grain average	4% plag, 10% ol	1,287	1,410	46.0
		1	Grain average	23% ol	1,082	470	12.8
		1	Grain average	10% ol	1,280	1,370	44.7
		1	Grain average	4% plag	1,349	1,790	58.2
		2	Grain average	4% plag, 23% ol	1,065	240	6.7
		2	Grain average	4% plag, 10% ol	1,259	1,130	31.0
		2	Grain average	23% ol	1,061	230	6.4
		2	Grain average	10% ol	1,253	1,090	29.9
		2	Grain average	4% plag	1,319	1,480	48.2
		3	Grain average	4% plag, 23% ol	1,068	280	7.6
		3	Grain average	4% plag, 10% ol	1,262	1,160	32.0
		3	Grain average	23% ol	1,064	260	7.2
		3	Grain average	10% ol	1,256	1,130	30.9
		3	Grain average	4% plag	1,323	1,520	49.5
		3	Grain average	4% plag, 23% ol	1,097	610	16.9
		3	Grain average	23% ol	1,093	600	16.5
		3	Grain average	10% ol	1,294	1,540	50.0
		3	Grain average	4% plag	1,364	1,960	63.8
		3	Grain average	4% plag, 10% ol	1,301	1,580	51.3
	B-4	1	Grain average	9% plag, 8% ol	1,240	1,050	28.7
		1	Grain average	9% plag	1,302	1,380	44.8
		1	Grain average	8% ol	1,227	990	27.1
		2	Grain average	9% plag, 8% ol	1,262	1,290	42.1
		2	Grain average	9% plag	1,326	1,640	53.4
		2	Grain average	8% ol	1,248	1,230	40.0
Coso	CQ-1	1	Grain average	19% plag, 5% ol	1,226	1,060	29.1
		1	Grain average	19% plag	1,271	1,290	41.9
		1	Grain average	5% ol	1,199	930	25.6
	CQ-2	1	Grain average	15% plag, 5% ol	1,193	700	19.4
		1	Grain average	15% plag	1,240	930	25.6
		1	Grain average	5% ol	1,174	630	17.3
		2	Grain average	15% plag, 5% ol	1,200	750	20.7
		2	Grain average	15% plag	1,248	980	27.0
		2	Grain average	5% ol	1,181	680	18.6
	CT-2	1	Grain average	16% plag, 4% ol	1,140	360	9.9
		1	Grain average	16% plag	1,191	570	15.7
		1	Grain average	4% olivine	1,120	300	8.2
		2	Sector A	16% plag, 4% ol	1,137	330	8.9
		2	Sector A	16% plag	1,187	530	14.7
		2	Sector A	4% olivine	1,117	260	7.2
		3	Sector A	16% plag, 4% ol	1,147	460	12.7
		3	Sector A	16% plag	1,199	680	18.7
		3	Sector A	4% olivine	1,127	400	11.0

Weight percentages of phenocrysts from modal data in ESM Table 1

average pressure of pyroxene crystallization of Big Pine basalts is 1.44 GPa. The average pressures of pyroxene crystallization of Coso Pliocene and Pleistocene basalts are 530 and 900 MPa, respectively. If magma erupts directly from depth without stalling in the crust, one would expect the pressure of crystallization of that magma to be similar to the pressure of crystallization of the source rock. The finding that the average pressure of pyroxene crystallization in Big Pine basalts is similar to the range of pressures of crystallization of the mantle xenoliths—the source rock for the basalts—is consistent with the hypothesis that Big Pine basalts erupted directly from depth without first stalling in the crust. Similarly, the observation that the average pressures of pyroxene crystallization of Coso basalts is shallower than the crystallization pressures of the mantle xenoliths is consistent with the hypothesis that Coso basalts stalled in the crust before erupting.

The calculated temperatures and pressures of basalt crystallization also agree well with seismic and heat flow studies at Coso. These studies suggest the presence of partially molten rock at a depth between 5 and 20 km (Combs 1980; Duffield et al. 1980; Reasenberg et al. 1980; Bacon 1982; Bacon et al. 1984; Manley and Bacon 2000; Wilson et al. 2003).

Manley and Bacon (2000) determined the depth to the top of the Coso rhyolite reservoir to be $\sim 5.5-10$ km. Although they do not make any estimates as to the thickness of the rhyolite magma body, the fact that the depth to rhyolite crystallization is shallower than that of

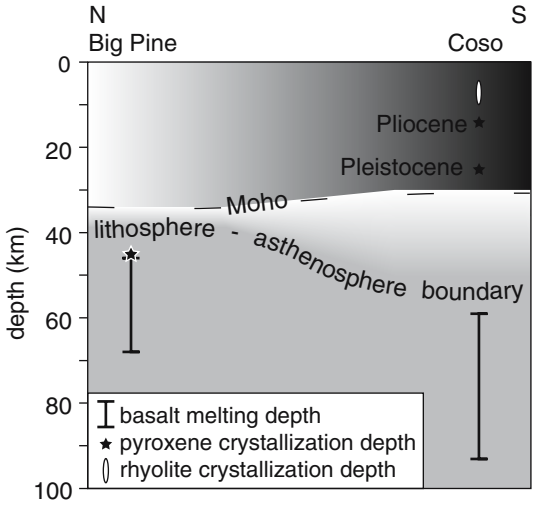

Fig. 5 Simplified model of the subsurface beneath Coso and Big Pine volcanic fields. The average depth to the Moho is from Fliedner et al. (1996), Ruppert et al. (1998), and Wang et al. (2002). The average depth to the lithosphere–asthenosphere boundary is from Jones et al. (1992) and Wang et al. (2002). Melting depths are from Wang et al. (2002). Average crystallization depths are from this study and Manley and Bacon (2000)

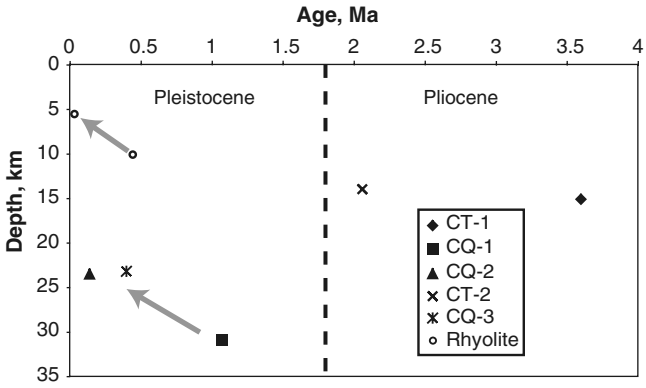

Fig. 6 Age versus crystallization depth of Coso basalts. Manley and Bacon (2000) found that depth to Pleistocene rhyolite storage decreased with time. The deepest Pleistocene Coso basalt is also the oldest but more data would need to be gathered to determine whether the depth to basalt storage also decreased with time

basalt crystallization is consistent with the hypothesis that rhyolite is present at Coso because basalt stalled in the crust and provided the heat necessary for melting.

Manley and Bacon (2000) showed that from 0.6 to 0.3 m.y. the depth to the top of the rhyolite magma body was ~ 10 km and by 0.04 m.y. it had risen to ~ 5.4 km. At the Coso volcanic field the oldest Pleistocene sample records the greatest crystallization depth and the two younger basalt samples record significantly shallower depths (Fig. 6), but inferring a shallowing trend would require more data.

Hypotheses on the differing magmatic processes at Coso and Big Pine

Results of this study indicate that Coso basalts crystallized pyroxene phenocrysts at crustal depths, whereas Big Pine basalts crystallized pyroxene phenocrysts at mantle depths. These calculations are consistent with the presence of abundant rhyolite at Coso and its near absence at Big Pine, and with the presence of mantle xenoliths at Big Pine and their absence at Coso. The question remains: what caused basalt to be trapped in the crust in the Coso field and not in the Big Pine field? Comparison of crystallization depths with crustal structure may provide a key.

Crystallization depths of clinopyroxene in Coso Pliocene basalts define a nearly isobaric trend on a plot of temperature vs. depth (Fig. 2a). Putirka and Condit (2003) found a similar trend in basalts from the Springerville volcanic field and interpreted it as an expression of depth of magma storage, where magma cooled isobarically. Data for Pleistocene Coso basalts tend to cluster, and at Big Pine temperature and depth of pyroxene crystallization are correlated over a broad range (Fig. 2a). These trends support the hypothesis that Coso basalts stalled in the crust whereas Big Pine basalts erupted directly from a range of mantle depths.

A mid-crustal positive P-wave velocity anomaly is present beneath the Coso volcanic field at a depth of approximately 15 km (Ruppert et al. 1998; Wilson et al. 2003). Glazner and Ussler (1988) noted that correlation of V_p with crustal density could indicate that crust above the density discontinuity is equally or less dense than typical basaltic magma and crust below the discontinuity more dense. Consequently, basaltic magma would be buoyant in the lower crust but not in the upper crust. Glazner and Ussler (1988) suggest that this could provide a trapping mechanism for mafic magma. The average depth of Coso Pliocene basalt storage (~ 14.5 km) corresponds well with the mid-crustal density discontinuity (~ 15 km), indicating that this is a possible trapping mechanism.

Bacon et al. (1981) suggested that Coso Pleistocene basalt, which likely provided the heat to generate Pleistocene rhyolite, may have been trapped beneath the Pliocene magma body, explaining why the former basalts record greater crystallization depths than the latter (~ 25 km vs. ~ 14.5 km, respectively).

An alternative trapping mechanism could be a rheology contrast in the mid-crust similar to that proposed by Putirka and Condit (2003) for the Springerville volcanic field. The results of the Southern Sierra Continental Dynamics project (Ruppert et al. 1998) show a change in P-wave velocity at approximately 25 km depth beneath Coso which is the average crystallization depth of Coso Pleistocene basalts, suggesting that a similar rheology contrast may be present at the Coso volcanic field. However, this feature is also present under the Big Pine field. Some combination of crustal density structure (Glazner and Ussler 1988; Black et al. 2002) and crustal

rheology likely prevented Coso basaltic magma from erupting directly from depth and consequently producing the geothermal field.

Conclusions

We determined the effects of analytical error, crystal zoning, and correlated errors on estimated temperatures and pressures from the thermobarometer of Putirka et al. (1996) and find them relatively small compared to intersample differences. Coso basalts record significantly shallower, intracrustal pyroxene crystallization depths than Big Pine basalts, which crystallized pyroxene in the mantle, supporting the hypothesis that basaltic magma stalled in the crust at Coso whereas basalt erupted directly from mantle depths at Big Pine. Coso basalts also record deeper crystallization depths than the eruptive depths of Coso rhyolites, supporting the hypothesis that basaltic magma provided the heat source to generate and sustain the rhyolite magma body.

Long residence times of basaltic magma are required to generate silicic and intermediate magma. Rhyolite is absent at Big Pine because basaltic magma did not stall in the crust, or did not stall long enough to generate silicic magma. Factors that allowed basalt to stall in the crust at Coso but erupt directly from depth at Big Pine likely include differences in crustal density and rheology.

Acknowledgments Research in the Coso field has been aided over the years by the U.S. Navy's Geothermal Program Office. We especially thank Frank Monastero for encouragement, expert advice, and a thorough technical review of this manuscript. Keith Putirka and Gordon Moore provided constructive and positive reviews for the journal, and Putirka helped us to properly implement the thermobarometer. Pre-submission reviews by Drew Coleman and Larry Benninger greatly aided the science and presentation. We thank Alan Boudreau for help with the microprobe analyses.

References

Bacon CR (1982) Time-predictable bimodal volcanism in the Coso range California. Geology 10:65–69

Bacon CR, Metz J (1984) Magmatic inclusions in rhyolites, contaminated basalts, and compositional zonation beneath the Coso volcanic field, California. Contrib Mineral Petrol 85:346–365

Bacon CR, MacDonald R, Smith RL, Baedecker PA (1981) Pleistocene high-silica rhyolites of the Coso volcanic field, Inyo county, California. J Geophys Res 86:10223–10241

Bacon CR, Kurasawa H, Delevaux MH, Kistler RW, Doe BR (1984) Lead and strontium isotopic evidence for crustal interaction and compositional zonation in the source regions of Pleistocene basaltic and rhyolitic magmas of the Coso volcanic field, California. Contrib Mineral Petrol 85:366–375

Bateman PC (1965) Geologic map of the Big Pine 15-minute quadrangle, California. U.S. Geol Surv Prof Pap 470, Plate 4

Beard BL, Glazner AF (1995) Trace element and Sr and Nd isotopic composition of mantle xenoliths from the Big Pine volcanic field, California. J Geophys Res 10:4169–4179

Bierman P, Gillespie A, Whipple K, Clark D (1991) Quaternary geomorphology and geochronology of Owens Valley, California: Geological Society of America field trip. In: Walawender MJ, Hanan BB (eds) Geological excursions in southern California and Mexico: guidebook for the 1991 annual meeting. Geological Society of America, San Diego, pp 199–223

Black RA, Walker JD, Baker GS (2002) Three-dimensional gravity modeling and crustal-density variations, Panamint Range to the eastern Sierra Nevada, southeastern California. Geol Soc Am Mem 195:229–241

Combs J (1980) Heat flow in the Coso geothermal area, Inyo County, California. J Geophys Res 85:2411–2424

Darrow AC (1972) Origin of the basalts of the Big Pine volcanic field, California. M.S. thesis, University of California, Santa Barbara

Ducea MN, Saleeby JB (1996) Buoyancy sources for a large, unrooted mountain range, the Sierra Nevada, California: evidence from xenolith thermobarometry. J Geophys Res 101:8229–8244

Duffield WA, Bacon CR, Dalrymple GB (1980) Late Cenozoic volcanism, geochronology, and structure of the Coso range, Inyo county, California. J Geophys Res 85:2381–2404

Fliedner MM, Ruppert S, SSCD Working Group (1996) Three-dimensional crustal structure of the southern Sierra Nevada from seismic fan profiles and gravity modeling. Geology 24:367–370

Glazner AF, Miller JS (1997) A major lithospheric boundary in eastern California defined by isotope ratios in Cenozoic basalts from the Coso Range and surrounding areas. Geol Soc Am Abs Programs 29:69

Glazner AF, Ussler W III (1988) Trapping of magma at midcrustal density discontinuities. Geophys Res Lett 15:673–675

Jensen BB (2000) Partitioning of elements in sector-zoned clinopyroxenes. Mineral Mag 64:725–728

Jones CH, Wernicke BP, Farmer GL, Walker JD, Coleman DS, McKenna LW, Perry FV (1992) Variations across and along a major continental rift: an interdisciplinary study of the Basin and Range Province, western USA. Tectonophysics 213:57–96

Lachenbruch AH, Sass JH (1978) Models of an extending lithosphere and heat flow in the Basin and Range province. Geol Soc Am Mem 52:209–250

Manley CR, Bacon CR (2000) Rhyolite thermobarometry and the shallowing of the magma reservoir, Coso volcanic field, California. J Petrol 41:149–174

Marsh BD (1981) On the crystallinity, probability of occurrence, and rheology of lava and magma. Contrib Mineral Petrol 78:85–98

McKenzie D, Bickle MJ (1988) The volume and composition of melt generated by extension of the lithosphere. J Petrol 29:625–679

Miller JS (1999) Recent perspectives on the dynamics of small-volume rhyolite magma systems from Coso volcanic field, CA. EOS Trans AGU 80:F1178

Miller JS, Wooden JL (2004) Residence, resorption and recycling of zircons in Devils Kitchen rhyolite, Coso volcanic field, California. J Petrol 45:2155–2170

Monastero FC, Katzenstein AM, Miller JS, Unruh JR, Adams MC, Richards-Dinger K (2005) The Coso geothermal field: a nascent metamorphic core complex. Geol Soc Am Bull 117:1534–1553

Moore JG (1963) Geology of the Mount Pinchot quadrangle southern Sierra Nevada California. US Geol Surv Bull 1130, Plate 1

Nakamura Y (1973) Origin of sector-zoning of igneous clinopyroxenes. Am Mineral 58:986–990

Nelson CA (1966) Geologic map of the Waucoba Mountain quadrangle, Inyo County, California. US Geological Survey Geologic Quadrangle Map GQ-528

Novak SW, Bacon CR (1986) Pliocene volcanic rocks of the Coso range, Inyo County, California. USGS special paper 1383, p 42

Ormerod DS, Hawkesworth CJ, Rogers NW, Leeman WP, Menzies MA (1988) Tectonic and magmatic transitions in the Western Great Basin, USA. Nature 333:349–353

Ormerod DS, Rogers NW, Hawkesworth CJ (1991) Melting in the lithospheric mantle: inverse modeling of alkali-olivine basalts from the Big Pine Volcanic Field, California. Contrib Mineral Petrol 108:305–317

Plouff D, Isherwood WF (1980) Aeromagnetic and gravity surveys in the Coso Range, California. J Geophys Res 85:2491–2501

Putirka K, Condit CD (2003) Cross section of a magma conduit system at the margin of the Colorado Plateau. Geology 31:701–704

Putirka K, Johnson M, Kinzler R, Longhi J, Walker D (1996) Thermobarometry of mafic igneous rocks based on clinopyroxene–liquid equilibria, 0–30 kbar. Contrib Mineral Petrol 123:92–108

Reasenberg PA, Ellsworth WL, Walter AW (1980) Teleseismic evidence for a low-velocity body under the Coso geothermal area. J Geophys Res 85:2471–2483

Ross DC (1965) Geology of the Independence quadrangle, Inyo County, California. U.S. Geol Surv Bull 1181-O

Ruppert S, Fliedner MM, Zandt G (1998) Thin crust and active upper mantle beneath Southern Sierra Nevada in the western United States. Tectonophysics 286:237–252

Steltenpohl MG, Bartley JM (1987) Thermobarometric profile through the Caledonian nappe stack of Western Ofoten, North Norway. Contrib Mineral Petrol 96:93–103

Takahashi E, Kushiro I (1983) Melting of a dry peridotite at high pressures and basalt magma genesis. Am Mineral 68:859–879

Tsuruta K, Takahashi E (1998) Melting study of an alkali basalt JB-1 up to 12.5 GPa: behavior of potassium in the deep mantle. Phys Earth Planet Inter 107:119–130

Walker JD, Black RA, Berry AK, Davis PJ, Andrew JE, Mitsdarfer JM (2002) Geologic maps of the northern Mojave Desert and southwestern Basin and Range Province, California; explanation of maps on CD-ROM. Geol Soc Am Mem 195:297–299

Wang K, Plank T, Walker JD, Smith EI (2002) A mantle melting profile across the Basin and Range, SW USA. J Geophys Res 107. DOI 10.1029/2001JB000209 ECV 5-1-21

Wilson CK, Jones CH, Gilbert HJ (2003) Single-chamber silicic magma system inferred from shear wave discontinuities of the crust and uppermost mantle, Coso geothermal area, California. J Geophys Res 108. DOI 10.1029/2002JB001798 ESE 2-1-16